2016 IEEE International Conference on Robotics and Automation (ICRA)
Stockholm, Sweden, May 16-21, 2016

A controllable flying vehicle with a single moving part

Weixuan Zhang, Mark W. Mueller, and Raffaello D'Andrea

Abstract— **This paper presents the "monospinner": a mechanically simple flying vehicle with only one moving part. The vehicle is shown to be controllable in three translational degrees of freedom and two rotational degrees of freedom. The vehicle has a single scalar control input, the thrust magnitude, and is controlled by a cascaded control strategy with an inner attitude controller and an outer position controller. The vehicle design is chosen based on two robustness metrics: the ability to maintain hover under perturbations and the probability of input saturation based on a stochastic model. The resulting mechanical and control designs are experimentally demonstrated, where it is also shown that the vehicle is sufficiently robust to achieve hover after being thrown into the air.**

I. Introduction

Highly underactuated flying vehicles present an interesting area of research, especially with respect to their control. The first category is the samara-type vehicle, which can be traced back to the 1950's [1]. They often have two actuators and are controllable in three translational degrees of freedom. Inspired by the maple seed (or samaras), the whole body resembles the look of the samara and rotates while flying. They are passively stable in attitude [2] and thus require no active attitude control to hover. The propulsion for the body rotation typically comes from a small propeller installed at one end of the body. Position control is achieved by varying the angle of the servo-driven control surface, similar to an aileron. Notable references are [3], [4], [5].

The second category is the passively stable vehicle with a single propeller. They have one actuator and no control surfaces. They are controllable in height, but not in the horizontal plane. They are also passively stable in attitude and capable of hovering flight without active attitude control. One such vehicle [6] has a single propeller producing thrust in the upright direction and is mounted with an aerodynamic damper. Similar vehicles exist as toys, for example the Air Hogs Vectron [7].

The third category is the flapping-wing flying vehicle. Those with one actuator use aerodynamic dampers to have passive stability in attitude and are only controllable in height [8], [9]. If they have two actuators (e.g. two wings are separately actuated), they may be controllable in the horizontal direction [10].

The fourth category is the ducted fan vehicle, having for example one rotating propeller. Such a vehicle is controllable in three translational degrees of freedom by having control authority over several control surfaces [11].

The authors are with the Institute for Dynamic Systems and Control, ETH Zurich, Sonneggstrasse 3, 8092 Zurich, Switzerland.
{wzhang, mwm, rdandrea}@ethz.ch

Multicopters (whose only inputs are fixed-pitch propellers with parallel axes of rotation) form the fifth category, with quadrocopters being the most popular. In [13], [14] it is shown that a quadrocopter can maintain flight despite the complete loss of two propellers (that is, with only two propellers remaining). It is also shown, theoretically, that control is possible after the complete loss of three propellers, however experimental validation was not done due to practical difficulties. This paper builds on these results, and presents a mechanically simple flying vehicle (called the "monospinner", and shown in Fig. 1) with only one moving part (the rotating propeller). The vehicle features no additional actuators or aerodynamic surfaces. This vehicle is controllable in three translational degrees of freedom and two attitude degrees of freedom.

This paper is organized as follows: Section II presents the dynamic modelling and hover solution of the monospinner. Section III then outlines the control strategy, while Section IV describes the design procedure. Section V presents the resulting vehicle. Section VI shows the experimental results, and the paper concludes in Section VII.

II. Modelling

This section presents the translational and rotational dynamics, followed by the hover solution of the vehicle.

A. Dynamic model

This model is adapted from [14] and specialized here for the monospinner. Fig. 2 shows some of the salient forces and

Fig. 1. The monospinner: a controllable flying vehicle with a single moving part. The vehicle is approximately 40 cm in size, the frame consists of five carbon-fiber plates, and the electronics are mounted in an aluminium cage inspired by the AscTec Hummingbird [12]. The carbon fiber rods help to protect the propeller during landing. A more detailed list of components is given in Table I.

978-1-4673-8025-6/16/$31.00 ©2016 IEEE

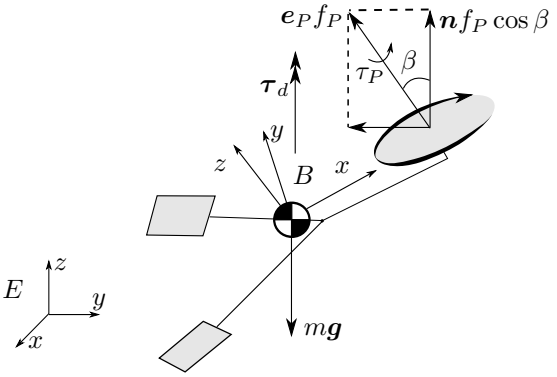

Fig. 2. Monospinner in flight, showing some of the symbols and quantities required to model the system.

quantities used in this section. The vehicle has a total mass m, and the gravity vector is denoted as $\boldsymbol{g}$. Boldface symbols like $\boldsymbol{g}$ are used throughout the paper to denote quantities in three-dimensional space. The propeller on the vehicle has only one degree of freedom (its rotation), and it produces a thrust force of magnitude f_P in the direction of the unit vector $\boldsymbol{e}_P$. The position of the vehicle's center of mass with respect to a point fixed in the inertial coordinate system is denoted as $\boldsymbol{p}$.

Two coordinate systems are used for the modelling: an inertial (ground-fixed) coordinate system E and a body-fixed coordinate system B. A vector expressed in a specific coordinate system is indicated by a superscript, for example $\boldsymbol{g}^E$ expresses $\boldsymbol{g}$ in coordinate system E. The coordinate system B is oriented such that the motor arm points in the direction $(1,0,0)$ from the center of mass and $\boldsymbol{e}_P^B = (0,0,1)$. The notation $(0,0,1)$ is used throughout this paper to compactly express the elements of a column vector.

The translational dynamics of the vehicle, expressed in the inertial system E, are captured by Newton's law:

$$m\ddot{\boldsymbol{p}}^E = \boldsymbol{e}_P^E f_P + m\boldsymbol{g}^E \tag{1}$$

where it is assumed that the vehicle travels at low translational velocities, such that translational drag forces (such as those described in [15]) are neglected.

The mass moment of inertia of the vehicle excluding the propeller (with respect to the vehicle's center of mass) is $\boldsymbol{I}_B$, and that of the propeller is $\boldsymbol{I}_P$. The vehicle rotates at an angular velocity $\boldsymbol{\omega}_{BE}$ with respect to the coordinate system E, where the subscript BE means the relative velocity of coordinate system B with respect to E. The propeller is located at a displacement $\boldsymbol{r}_P$ with respect to the center of mass, and its angular velocity with respect to the coordinate system E is denoted as $\boldsymbol{\omega}_{PE}$. Besides the thrust f_P, the propeller also produces a reaction torque of magnitude τ_P in the propeller thrust direction $\boldsymbol{e}_P$. The vehicle experiences an airframe drag torque $\boldsymbol{\tau}_d$ due to the rotation of the vehicle in the air.

Using Euler's law, the attitude dynamics expressed in the body-fixed coordinate system B are formulated as:

$$\boldsymbol{I}_B^B\dot{\boldsymbol{\omega}}_{BE}^B + \boldsymbol{I}_P^B\dot{\boldsymbol{\omega}}_{PE}^B + [\![\boldsymbol{\omega}_{BE}^B\times]\!](\boldsymbol{I}_B^B\boldsymbol{\omega}_{BE}^B + \boldsymbol{I}_P^B\boldsymbol{\omega}_{PE}^B) = [\![\boldsymbol{r}_P^B\times]\!]\boldsymbol{e}_P^B f_P + \boldsymbol{e}_P^B\tau_P + \boldsymbol{\tau}_d^B \tag{2}$$

where $[\![\boldsymbol{a}\times]\!]$ represents the skew-symmetric matrix form of the cross product, so that $[\![\boldsymbol{a}\times]\!]\mathbf{b} = \mathbf{a}\times\mathbf{b}$ for any 3D vectors $\mathbf{a}$ and $\mathbf{b}$.

The propeller's scalar speed Ω with respect to the body is usually controlled by an electronic speed controller, so that

$$\boldsymbol{\omega}_{PB}^B = (0,0,\Omega). \tag{3}$$

Note that $\boldsymbol{\omega}_{PE}^B$ can be decomposed as below:

$$\boldsymbol{\omega}_{PE}^B = \boldsymbol{\omega}_{PB}^B + \boldsymbol{\omega}_{BE}^B. \tag{4}$$

The thrust f_P and the torque τ_P produced from a stationary propeller are assumed to be proportional to its angular velocity $\boldsymbol{\omega}_{PE}^B$ squared with the proportional coefficients κ_f and κ_τ, respectively [16]:

$$f_P = \kappa_f(\boldsymbol{\omega}_{PE}^B\cdot\boldsymbol{e}_P^B)|\boldsymbol{\omega}_{PE}^B\cdot\boldsymbol{e}_P^B| \tag{5}$$

$$\tau_P = -\kappa_\tau(\boldsymbol{\omega}_{PE}^B\cdot\boldsymbol{e}_P^B)|\boldsymbol{\omega}_{PE}^B\cdot\boldsymbol{e}_P^B| \tag{6}$$

with $\cdot$ denoting the vector inner product. Note that by substituting (3) into (4) and the resulting equation into (5) and (6), f_P and τ_P are uniquely defined by Ω and $\boldsymbol{\omega}_{BE}^B$.

It is assumed that the magnitude of the airframe drag torque $\boldsymbol{\tau}_d$ is quadratic in the vehicle's angular velocity $\boldsymbol{\omega}_{BE}^B$ [14]:

$$\boldsymbol{\tau}_d^B = -\left\|\boldsymbol{\omega}_{BE}^B\right\|\boldsymbol{K}_d^B\boldsymbol{\omega}_{BE}^B \tag{7}$$

where $\|\cdot\|$ denotes the Euclidean norm and $\boldsymbol{K}_d^B$ is assumed to be a diagonal 3×3 matrix in the coordinate system B, which is denoted by

$$\boldsymbol{K}_d^B = \mathrm{diag}\left(K_{d,xx}, K_{d,yy}, K_{d,zz}\right). \tag{8}$$

B. Hover solution

The hover solution of the monospinner follows the definition of the "relaxed hover solutions" [14], which are defined as solutions that are constant when expressed in a body-fixed reference frame and where the vehicle remains substantially in one position. Specifically, these solutions allow the vehicle to have a non-zero angular velocity.

In hover, the monospinner's center of mass has a uniform circular motion at a constant height, while the vehicle body is rotating at a constant angular velocity $\bar{\boldsymbol{\omega}}_{BE}^B$ in the parallel direction of gravity. Note that the overbar in this paper is always used to denote quantities that are constant in hover (i.e. the equilibrium solution). Although the vehicle's attitude is constantly changing due to the non-zero angular velocity, there exists a body-fixed unit vector $\boldsymbol{n}$, which does not change when expressed in the coordinate system E. This vector may be thought as an averaged thrust direction of the vehicle – note that the instantaneous thrust direction may not be aligned with gravity.

The dynamics of a vector $\boldsymbol{l}$ expressed in two different coordinate systems are described as [17]

$$\dot{\boldsymbol{l}}^B = -[\![\boldsymbol{\omega}_{BE}^B\times]\!]\boldsymbol{l}^B + \boldsymbol{C}^{BE}\dot{\boldsymbol{l}}^E \tag{9}$$

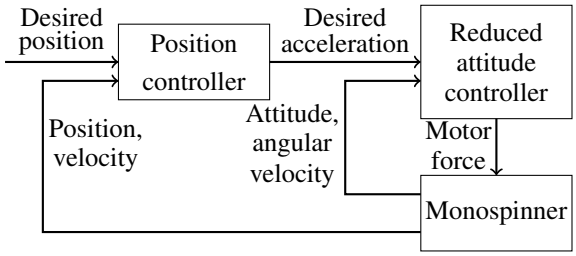

Fig. 3. Cascaded control structure: the outer position controller defines a desired acceleration, where the inner attitude controller defines the vehicle's attitude.

where $\boldsymbol{C}^{BE}$ is the coordinate transformation matrix from the coordinate system E to the coordinate system B.

The averaged thrust direction $\boldsymbol{n}$ is constant in hover, such that $\dot{\boldsymbol{n}}^B = 0$ and $\dot{\boldsymbol{n}}^E = 0$, which leads to $[\![\bar{\boldsymbol{\omega}}^B_{BE}\times]\!]\boldsymbol{n}^B = 0$ according to (9). Assuming $\bar{\boldsymbol{\omega}}^B_{BE} \neq 0$, this implies that

$$\boldsymbol{n}^B = \pm\frac{\bar{\boldsymbol{\omega}}^B_{BE}}{\left\|\bar{\boldsymbol{\omega}}^B_{BE}\right\|} \tag{10}$$

where the sign is chosen such that $\boldsymbol{n}$ points upwards in the inertial coordinate system.

The equilibrium propeller force $\boldsymbol{e}^B_P\bar{f}_P$ can be decomposed into the horizontal and the vertical force, where the horizontal force induces the circular motion and the vertical force compensates for the vehicle's weight. The angle β in Fig. 2 is the angle between the propeller force direction $\boldsymbol{e}^B_P$ and the averaged thrust direction $\boldsymbol{n}^B$ (where $\boldsymbol{n}$ is vertical according to (10)). Then

$$\cos(\beta) = \boldsymbol{e}^B_P\boldsymbol{n}^B \tag{11}$$

and the vertical component of the equilibrium propeller force on the vertical direction is:

$$\bar{f}_P\cos(\beta) = m\left\|\boldsymbol{g}\right\|. \tag{12}$$

Substituting (10) into (11), and then substituting the resulting equation into (12), yields the following solution for the equilibrium thrust

$$\bar{f}_P = \frac{m\left\|\boldsymbol{g}\right\|\left\|\bar{\boldsymbol{\omega}}^B_{BE}\right\|}{|\boldsymbol{e}^B_P\bar{\boldsymbol{\omega}}^B_{BE}|}. \tag{13}$$

In hover (i.e. setting the derivatives to zero), (2) becomes:

$$[\![\bar{\boldsymbol{\omega}}^B_{BE}\times]\!](\boldsymbol{I}^B_B\bar{\boldsymbol{\omega}}^B_{BE} + \boldsymbol{I}^B_P\bar{\boldsymbol{\omega}}^B_{PE}) = [\![\boldsymbol{r}^B_P\times]\!]\boldsymbol{e}^B_P\bar{f}_P + \boldsymbol{e}^B_P\bar{\tau}_P + \bar{\boldsymbol{\tau}}^B_d. \tag{14}$$

Note that the quantities $\bar{\boldsymbol{\omega}}^B_{PE}$, $\bar{f}_P$, $\bar{\tau}_P$ and $\bar{\boldsymbol{\tau}}_d$ are uniquely defined by $\bar{\Omega}$ and $\bar{\boldsymbol{\omega}}^B_{BE}$ (see (3), (4), (5), (6), (7)), such that we have four equations in four unknowns. The hover solution is therefore defined by the $\bar{\Omega}$ and $\bar{\boldsymbol{\omega}}^B_{BE}$ that solve (13)-(14). With the resulting $\bar{\Omega}$ and $\bar{\boldsymbol{\omega}}^B_{BE}$ all other quantities in hover (such as $\boldsymbol{n}^B$ or $\bar{f}_P$) may be calculated.

III. Control strategy

The monospinner employs a cascaded control strategy, where the outer loop is a position controller and the inner loop is an attitude controller (see Fig. 3).

A. Position control

The position error of the vehicle (i.e. the vector to a desired point in space) is defined as $\boldsymbol{p}^E$, and its velocity error as $\dot{\boldsymbol{p}}^E$, where both are expressed in the inertial coordinate system. A desired acceleration command $\ddot{\boldsymbol{p}}^E_{\mathrm{des}}$ is calculated as follows:

$$\ddot{\boldsymbol{p}}^E_{\mathrm{des}} = -2\zeta\omega_n\dot{\boldsymbol{p}}^E - \omega_n^2\boldsymbol{p}^E \tag{15}$$

where ζ is a damping ratio and ω_n is a natural frequency. If $\ddot{\boldsymbol{p}}^E_{\mathrm{des}}$ can be tracked perfectly, the translational deviation $\boldsymbol{p}^E$ will behave like a damped second-order system. This acceleration command is used as input by the attitude controller.

The magnitude of the thrust force required by the position control f_{pos}, and the desired averaged thrust direction $\boldsymbol{n}^E_{\mathrm{des}}$, may be calculated from the desired acceleration as below, from (1)

$$\cos(\beta)\, f_{\mathrm{pos}}\boldsymbol{n}^E_{\mathrm{des}} = m(\ddot{\boldsymbol{p}}^E_{\mathrm{des}} - \boldsymbol{g}^E) \tag{16}$$

where $\cos(\beta)$ is the fraction of the propeller thrust in the averaged thrust direction from (11).

B. Reduced attitude control

The goal of the attitude controller is to control $\boldsymbol{n}^E$ to point along $\boldsymbol{n}^E_{\mathrm{des}}$ while producing the desired position control thrust f_{pos}. The control of a unit vector $\boldsymbol{n}^E$ is often called "reduced attitude control" [18].

For convenience a control coordinate system C is introduced which is fixed with respect to the body-fixed coordinate system B and where

$$\boldsymbol{n}^C = \boldsymbol{C}^{CB}\boldsymbol{n}^B = (0,0,1). \tag{17}$$

The goal of controlling $\boldsymbol{n}^E$ to $\boldsymbol{n}^E_{\mathrm{des}}$ is equivalently encoded in the control coordinates as controlling $\boldsymbol{n}^C_{\mathrm{des}}$ to $\boldsymbol{n}^C$. It is assumed that the inner attitude loop dynamics are much faster than those of the outer position control loop, such that $\boldsymbol{n}^E_{\mathrm{des}}$ may be taken as constant here, i.e. $\dot{\boldsymbol{n}}^E_{\mathrm{des}} = 0$. Then, according to (9), the dynamics for $\dot{\boldsymbol{n}}^B_{\mathrm{des}}$ are:

$$\dot{\boldsymbol{n}}^B_{\mathrm{des}} = -[\![\boldsymbol{\omega}^B_{BE}\times]\!]\boldsymbol{n}^B_{\mathrm{des}}. \tag{18}$$

1) Attitude control state vector: A six dimensional state vector is introduced, including two components of the averaged thrust direction, three components of angular velocity, and a motor force state. The averaged thrust direction components η_i are introduced, such that $\boldsymbol{n}^C_{\mathrm{des}} = (\eta_1, \eta_2, \eta_3)$, where only η_1 and η_2 are considered as the states in the attitude controller: this is because the unit vector has 2 degrees of freedom, and $\eta_3 = 1$ to first order near hover.

The three angular velocity components α_i are introduced as below:

$$\boldsymbol{\omega}^C_{BE} = \boldsymbol{C}^{CB}\boldsymbol{\omega}^B_{BE} = (\alpha_1, \alpha_2, \alpha_3) \tag{19}$$

where specifically by (10) and (17) the equilibrium angular velocity $\bar{\boldsymbol{\omega}}_{BE}$ expressed in coordinate system C is:

$$\bar{\boldsymbol{\omega}}^C_{BE} = \pm\boldsymbol{C}^{CB}\boldsymbol{n}^B\left\|\bar{\boldsymbol{\omega}}^B_{BE}\right\| = (0,0,\pm\left\|\bar{\boldsymbol{\omega}}^B_{BE}\right\|). \tag{20}$$

The motor dynamics may have a large influence on the attitude system, if the time constant of their response to commands is comparable to the time constants of the remainder

of the attitude system. For this reason the motor force is also included as a state, and is approximated by a first order system with time constant τ_{mot}:

$$\dot{f}_P = \tau_{\text{mot}}^{-1}(f_{\text{com}} - f_P) \tag{21}$$

where f_{com} is the command thrust for the propeller and f_P is the current propeller thrust.

Under the assumption that the position control is much slower than the attitude control so that f_{pos} is constant, u is introduced such that

$$u = f_{\text{com}} - f_{\text{pos}} \tag{22}$$

and (21) may be rewritten as

$$\dot{f}_P = \tau_{\text{mot}}^{-1}(f_{\text{pos}} - f_P + u). \tag{23}$$

The reduced attitude control can be formalized by introducing the state deviation from the hover solution:

$$s = (\eta_1, \eta_2, \alpha_1, \alpha_2, \alpha_3, f_P) - (0, 0, 0, 0, 0, \pm \left\|\bar{\boldsymbol{\omega}}_{BE}^{B}\right\|, \bar{f}_P). \tag{24}$$

The time derivative $\dot{s}$ follows from (18), (2) and (23) expressed in the coordinate system C. Defining u as the control input and linearizing the system around the hover solution yields a linear, time-invariant system as below, which may be used to establish controllability of the monospinner:

$$\dot{s} \approx As + Bu. \tag{25}$$

2) Attitude controller design: A linear quadratic regulator (LQR) is designed for (25), with cost on deviations from the desired unit vector set to $75\,\text{s}^{-1}$, cost on the angular velocity set to 0, cost on the motor thrust deviation set to 0 and cost on the input set to $1\,\text{N}^{-2}\,\text{s}^{-1}$, to yield a static feedback gain K:

$$u = -Ks. \tag{26}$$

Note that the resulting thrust command $f_{\text{com}} = f_{\text{pos}} + u$ is a compromise between the attitude control input u and the position control input f_{pos}.

IV. Design

Compared to the presented (ideal) model, the real system includes several uncertainties such as parametric uncertainties, unmodelled dynamics, and measurement noise. This section presents the approach used to find a vehicle configuration, such that the vehicle is sufficiently robust against these uncertainties. Two different ways of comparing vehicle configurations are presented: input saturation probability and Monte Carlo analysis, while μ-analysis [19] is briefly discussed.

A. Simplified mechanical model

To allow for efficient evaluation, a simplified mechanical model is used for the analysis, where there are three major components in the vehicle: the battery, the electronics and the motor (including the propeller). The components' contribution to the composite inertia matrix is approximated as follows: the three major components are approximated as point masses and the connecting frame components are approximated as thin rods. From the inertia matrix (and by assuming that the vehicle has similar drag coefficients as the quadrocopter in [20]), the resulting vehicle's equilibrium solution and the linearized system matrices can be computed as described in the preceding sections.

The battery is taken to have a weight of $0.06\,\text{kg}$, the electronics $0.045\,\text{kg}$ and the motor $0.04\,\text{kg}$. The connecting rods are taken to have a length density of $0.06\,\text{kg}\,\text{m}^{-1}$.

B. Choosing the vehicle configuration

The vehicle's approximate size and shape are based on the existing trispinner [14], with a Y-shape and a vehicle diameter of approximately 40 cm. The three major components are always taken to be coplanar and the positions of the battery and the motor are fixed to be two vertices of an equilateral triangle, while the position of the electronics is to be determined.

A 2-dimensional grid search of the position of the electronics is then conducted, where two different quality metrics are considered. The first is the probability of input saturation, and is based on the linear, time-invariant model of the attitude system. The second metric uses Monte Carlo simulations of the nonlinear system, including parameter perturbations and noise, to approximate the probability that the resulting vehicle is able to maintain a hover. The probability of input saturation may be computed in closed form for a given design and is therefore cheap to evaluate, but is less informative than the Monte Carlo simulations.

1) Probability of input saturation: It is important to know how measurement and process noises relate to the actual input force, specifically how likely they are to lead to input saturation. This is critical for the monospinner: because the vehicle is not passively stable, input saturation may quickly lead to a crash. Here, the linear-time invariant system presented previously is discretized in time and augmented with measurement and actuator noises as determined by dedicated experiments. The stochastic characteristics of the propeller force may then be calculated in closed-form.

Discretizing the system (25) with a zero-order-hold on the input $u[k]$ results in:

$$s[k+1] = A_d s[k] + B_d u[k] \tag{27}$$

where A_d and B_d are the discretized system matrices.

A five-dimensional measurement noise $w_{\text{meas}}[k]$ is introduced, assumed to be zero-mean, white, and Gaussian. The measurement $z[k]$ is obtained by:

$$z[k] = C_d s[k] + w_{\text{meas}}[k] \tag{28}$$

where all states except the current propeller force are directly measured

$$C_d = \begin{bmatrix} I_5 & \mathbf{0} \end{bmatrix} \tag{29}$$

where I_5 is the identity matrix and $\mathbf{0} \in \mathbb{R}^5$ is a zero column vector.

A steady-state Kalman filter yields a state estimate $\hat{s}[k]$:

$$\hat{s}[k] = (I_6 - K_f C_d)(A_d \hat{s}[k-1] + B_d u[k-1]) + K_f z[k] \tag{30}$$

where K_f is the filter gain. The controller input follows from applying the LQR gain (26) to the state estimate. However, since there is actuator noise $w_{\text{act}}[k]$ (assumed white, Gaussian, and zero-mean) in the system, the true control input $u_{\text{true}}[k]$ is:

$$u_{\text{true}}[k] = -K\hat{s}[k] + w_{\text{act}}[k]. \tag{31}$$

The extended state $\tilde{s}[k] = (s[k], \hat{s}[k])$ and noise $\tilde{w}[k] = (w_{\text{meas}}[k], w_{\text{act}}[k])$ are defined. Then, by using $u_{\text{true}}[k]$ instead of $u[k]$, substituting (28) into (30) (to eliminate $z[k]$) and defining the extended system matrices $\tilde{A}$, $\tilde{B}$, $\tilde{C}$ and $\tilde{D}$ from (27), (28), (30), and (31); the extended system equations are:

$$\tilde{s}[k+1] = \tilde{A}\tilde{s}[k] + \tilde{B}\tilde{w}[k] \tag{32a}$$

$$u_{\text{true}}[k] = \tilde{C}\tilde{s}[k] + \tilde{D}\tilde{w}[k]. \tag{32b}$$

Let $P_{\tilde{w}}$, $P_{\tilde{s}}$ and $P_{u_{\text{true}}}$ be the variables' associated steady-state covariance matrices (e.g. $P_{\tilde{s}} = \text{Var}\,(\tilde{s}[k])$ for $k \to \infty$). By computing the variance of both sides of (32a), and letting $k \to \infty$, the variance $P_{\tilde{s}}$ can be computed, which allows to compute $P_{u_{\text{true}}}$ using (32b):

$$P_{\tilde{s}} = \tilde{A}P_{\tilde{s}}\tilde{A}^T + \tilde{B}P_{\tilde{w}}\tilde{B}^T \tag{33a}$$

$$P_{u_{\text{true}}} = \tilde{C}P_{\tilde{s}}\tilde{C}^T + \tilde{D}P_{\tilde{w}}\tilde{D}^T. \tag{33b}$$

Since $P_{\tilde{w}}$ is known from experiment and $\tilde{A}$ and $\tilde{B}$ are known, $P_{\tilde{s}}$ can be solved by (33a). Substituting into (33b) gives the variance of the actuator $P_{u_{\text{true}}}$. Since the noise $\tilde{w}[k]$ is assumed Gaussian, $u_{\text{true}}[k]$ is also Gaussian.

Given its variance $P_{u_{\text{true}}}$ and the equilibrium thrust $\bar{f}_P$ (the Gaussian variable's mean), the probability of saturating the maximal allowed thrust at least once in 1000 time steps may be calculated. Note that this allows to capture the fact that a design with low variance may still have a high probability of saturation if it has a high mean thrust. The value of 1000 steps is chosen as it is equivalent to one second of flight on the experimental platform. In this way the saturation probability of varying positions of the electronics is computed and shown in Fig. 4, and the results are discussed below.

2) Monte Carlo analysis: For each position of the electronics, the nominal hover solution is solved for and an LQR controller is designed using the costs given in the preceding section: this controller is denoted as the "nominal controller". One hundred perturbed vehicles are then generated, by perturbing the following: inertia matrix $\boldsymbol{I}_B^B$, mass m, and drag coefficients $K_{d,xx}$, $K_{d,yy}$ and $K_{d,zz}$. Each of these parameters is perturbed by sampling within a certain percentage range of the nominal value. For each perturbed vehicle a nonlinear simulation is conducted, lasting 10 simulated seconds. In addition to the perturbed parameters, actuator noise and the measurement noises are simulated as in (28) and (31).

The perturbed vehicle starts at the reference position in the nominal hover state and is controlled by the nominal controller. If the vehicle has distance greater than 5 m from the reference position at the end of the simulation, it is counted as a failure case. For each candidate position of the electronics, the number of failure cases is plotted in Fig. 5. This number of failure cases is used as an indicator of the robustness of corresponding nominal configuration.

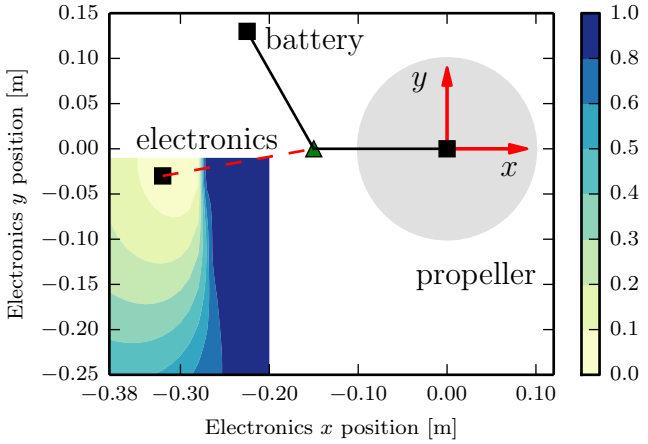

Fig. 4. The probability of the input saturation at least once during 1 second for varying position of the electronics. In the colored area, a grid search with resolution 0.01 m both in $\boldsymbol{x}$- and $\boldsymbol{y}$-direction is conducted. Note that a conservative saturation limit is chosen. The chosen position of the electronics is also plotted.

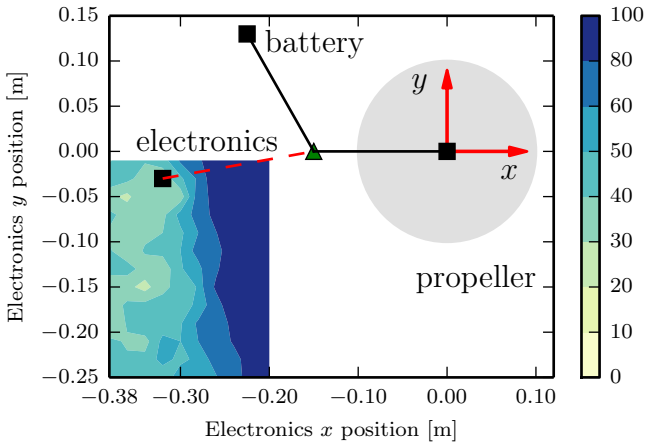

Fig. 5. The number of failure cases of vehicles under perturbations in nonlinear simulation for varying position of electronics. Note that a conservative set of perturbation range is chosen. The chosen position of the electronics is also plotted.

3) Discussion: Note that in both Figs. 5 and 4, there is a good, relatively flat, region of electronics position which has similar small number of failure cases (respectively a low probability of input saturation). The electronics' position was chosen as $(-0.32, -0.03, 0)$m in the coordinate system shown, based on good performance in both metrics, and a compromise with mechanical strength/complexity and the length of the cables required to connect the components.

C. μ-analysis

An alternative analysis tool to the preceding is μ-analysis [19], which aims to analyze whether a system is stable even under the worst-case disturbances and perturbations. However, this approach was found to be overly conservative,

TABLE I

COMPONENTS OF THE MONOSPINNER

Component	Name
Propeller	GEMFAN GF 8045
Motor	T-Motor MN2204-28 KV:1400
Motor controller	AutoQuad ESC32
Command radio	Laird RM024-S125-M-20
Flight controller	PX4FMU v1.7
Battery	G8 Pro Lite 480mAh 3-Cell/3S 11V
Power module	APM Power Module

and did not yield a useful vehicle configuration.

V. RESULTING VEHICLE

The resulting vehicle, as shown in Fig. 1, has a mass of $0.217\,\mathrm{kg}$ and moment of inertia as below (calculated from a CAD-model):

$$\boldsymbol{I}_B = \begin{bmatrix} 102 & 24 & 9 \\ 24 & 318 & 0 \\ 9 & 0 & 414 \end{bmatrix} \times 10^{-5}\,\mathrm{kg\,m^{-2}}. \tag{34}$$

The linearized system matrices are:

$$A = \begin{bmatrix} 0 & 23.7 & 0 & -1 & 0 & 0 \\ -23.7 & 0 & 1 & 0 & 0 & 0 \\ 0 & 0 & -2.4 & -9.5 & 5.2 & -25.7 \\ 0 & 0 & 17.0 & -0.4 & 10.8 & -58.8 \\ 0 & 0 & -1.8 & -6.3 & -1.0 & -1.7 \\ 0 & 0 & 0 & 0 & 0 & -18.2 \end{bmatrix} \tag{35}$$

$$B = \begin{bmatrix} 0 & 0 & 0 & 0 & 0 & 18.2 \end{bmatrix}^T. \tag{36}$$

It can be confirmed that the pair (A, B) is controllable, and the eigenvalues of the system matrix A are: $\{\pm 23.7j, -0.4 \pm 15.5j, -2.87, -18.2\}$. Note that it has two eigenvalues on the imaginary axis.

The expected hover solution for this vehicle is

$$\bar{\boldsymbol{\omega}}^B_{BE} = (7.0, -3.7, 22.4)\,\mathrm{rad\,s^{-1}} \tag{37}$$

$$\bar{f}_P = 2.26\,\mathrm{N}. \tag{38}$$

Table I lists the major components of the monospinner.

VI. EXPERIMENTAL VALIDATION

The mechanical and control designs are validated in experiment in the Flying Machine Arena (FMA) at ETH Zurich. An infrared motion capture system provides high-quality position and attitude measurements of the vehicle. The position control is run on a desktop computer at $50\,\mathrm{Hz}$, with commands transmitted wirelessly to the monospinner; the attitude control is run on-board the vehicle at $1000\,\mathrm{Hz}$. For more information on the FMA infrastructure, see [20]. The attached video illustrates the two types of experiments done: take-off from a platform and hand-launching (throwing) [1].

[1]A link is available on the authors' webpage

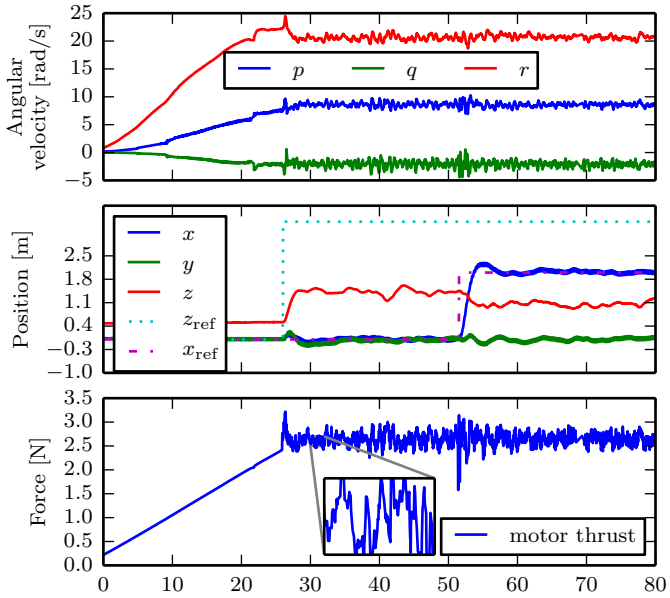

Fig. 6. Experimental results for the monospinner's take-off from the platform. The vehicle takes off at 26 s. At time 52 s, a reference position change of 2 m is set in the (horizontal) $\boldsymbol{x}$-direction. Note that at steady-state there is offset between the vehicle's height z and the reference height z_{ref}, this is due to the discrepancy between the expected hover solution and the true hover solution and it may be readily compensated by adding an integral term to the position control. The angular velocity is plotted as expressed in the body-fixed coordinate system, where $\boldsymbol{\omega}^B_{BE} = (p, q, r)$. The attached video shows such an experiment.

A. Take-off and hover

The vehicle takes off from a passive mechanism, designed to allow the vehicle achieve an angular velocity close to its equilibrium. The mechanism consists of a platform, on which the monospinner rests, connected by a bearing to the ground, so that the monospinner can freely rotate about its vector $\boldsymbol{n}$. The rotation is achieved solely through the reaction torque τ_P of the propeller, and the thrust is slowly ramped up from zero to the equilibrium solution. Once sufficiently close to equilibrium, the full control is switched on and the vehicle takes off. Fig. 6 shows the vehicle states during take-off, followed by approximately $25\,\mathrm{s}$ in hover, and then a horizontal step of $2\,\mathrm{m}$.

The hover solution the vehicle achieves in hover is as below, which may be compared to the expected values in (37) and (38)

$$\bar{\boldsymbol{\omega}}^B_{BE} = (8.7, -2.1, 20.4)\,\mathrm{rad\,s^{-1}} \tag{39}$$

$$\bar{f}_P = 2.32\,\mathrm{N}. \tag{40}$$

The discrepancy between the expected and the true hover solution has the effect that in reality the state deviation $\bar{s}$ in (24) and $\bar{u}$ are not zero in hover. In order to produce the correct thrust command $\bar{f}_{\mathrm{com}}$ for hovering (that is $\bar{f}_P$) the position controller has to result a $\bar{f}_{\mathrm{pos}}$ different than $\bar{f}_P$ according to (22), which means a constant position error in $\boldsymbol{z}$-direction is needed according to (15) and (16). This steady-state offset error is shown in Fig. 6.

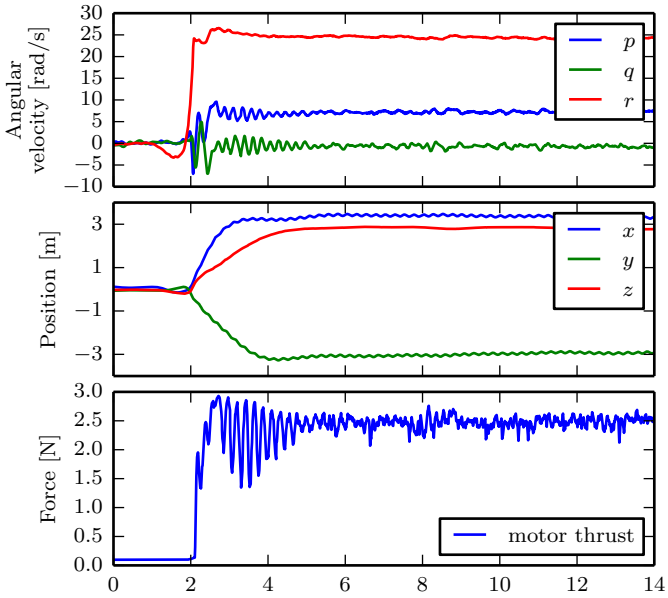

Fig. 7. Experimental results for the monospinner's hand launch. The vehicle is thrown at approximately 2 s, after which the controllers are switched on. The angular velocity is plotted as expressed in the body-fixed coordinate system, where $\boldsymbol{\omega}_{BE}^{B} = (p, q, r)$. The attached video shows such an experiment.

B. Hand launch

Alternatively, the monospinner may be launched by throwing it like a frisbee as shown in the attached video. This is a faster method of achieving hover than the takeoff mechanism in Section VI-A, and demonstrates the vehicle's ability to reject large disturbances. The state history during a representative hand launch is shown in Fig. 7.

Note that the hover solution in Fig.7 is different than the solution in Fig. 6:

$$\bar{\boldsymbol{\omega}}_{BE}^{B} = (7.3, -0.7, 24.3)\,\mathrm{rad\,s^{-1}} \quad (41)$$

$$\bar{f}_P = 2.22\,\mathrm{N}\,. \quad (42)$$

This is due to the slightly changed vehicle configuration, where one of the motion capture markers was moved.

VII. Conclusion

This paper presents a controllable flying vehicle with only one moving part and a single control input, which can fully control its position. Notably, stability is achieved through active control, rather than through **passive** aerodynamic effects. The mechanical design follows from a search over the parameter space, in an attempt to find a sufficiently robust design. The resulting vehicle is validated in experiments, wherein it is demonstrated that the vehicle can successfully hover, and has sufficient control authority to achieve a hover when hand-launched.

Acknowledgements

The authors would like to thank Michael Egli and Kiera van der Sande for the mechanical design of the monospinner and help with experiments. The authors would also like to thank Dario Brescianini and Boris Ivanovic for their helpful discussion on the AutoQuad 32 motor controller. The Flying Machine Arena is the result of contributions of many people, a full list of which can be found at `http://flyingmachinearena.org/`.

References

[1] C. McCutchen, "Flying machines," *Aeromodeller Magazine, July*, 1954.

[2] R. Norberg, "Autorotation, self-stability, and structure of single-winged fruits and seeds (samaras) with comparative remarks on animal flight," *Biological Reviews*, vol. 48, no. 4, pp. 561–596, 1973.

[3] J. Houghton and W. Hoburg, "Fly-by-wire control of a monocopter," Technical report, EECS, UC Berkley, Cambridge, MA, USA, Tech. Rep., 2008.

[4] E. R. Ulrich, D. J. Pines, and J. S. Humbert, "From falling to flying: the path to powered flight of a robotic samara nano air vehicle," *Bioinspiration & biomimetics*, vol. 5, no. 4, pp. 045 009–045 025, 2010.

[5] S. Jameson, K. Fregene, M. Chang, N. Allen, H. Youngren, and J. Scroggins, "Lockheed martin's samarai nano air vehicle: Challenges, research, and realization," in *50th AIAA Aerospace Sciences Meeting, January*, 2012, pp. 1–21.

[6] M. Piccoli and M. Yim, "Passive stability of a single actuator micro aerial vehicle," in *IEEE International Conference on Robotics and Automation (ICRA)*. IEEE, 2014, pp. 5510–5515.

[7] G. Richards, "Christmas under control!" *Engineering & Technology*, vol. 5, no. 18, pp. 42–43, 2010.

[8] Z. E. Teoh, S. B. Fuller, P. Chirarattananon, N. Prez-Arancibia, J. D. Greenberg, and R. J. Wood, "A hovering flapping-wing microrobot with altitude control and passive upright stability," in *IEEE/RSJ International Conference on Intelligent Robots and Systems (IROS)*. IEEE, 2012, pp. 3209–3216.

[9] F. Van Breugel, W. Regan, and H. Lipson, "From insects to machines," *Robotics & Automation Magazine, IEEE*, vol. 15, no. 4, pp. 68–74, 2008.

[10] K. Y. Ma, P. Chirarattananon, S. B. Fuller, and R. J. Wood, "Controlled flight of a biologically inspired, insect-scale robot," *Science*, vol. 340, no. 6132, pp. 603–607, 2013.

[11] E. N. Johnson and M. A. Turbe, "Modeling, control, and flight testing of a small-ducted fan aircraft," *Journal of guidance, control, and dynamics*, vol. 29, no. 4, pp. 769–779, 2006.

[12] "AscTec Hummingbird," (Date last accessed 15-Sept-2015). [Online]. Available: http://www.asctec.de/uav-uas-drohnen-flugsysteme/asctec-hummingbird/

[13] M. W. Mueller and R. D'Andrea, "Stability and control of a quadrocopter despite the complete loss of one, two, or three propellers," in *IEEE International Conference on Robotics and Automation (ICRA)*. IEEE, 2014, pp. 45–52.

[14] ——, "Relaxed hover solutions for multicopters: application to algorithmic redundancy and novel vehicles," *International Journal of Research Robotics*.

[15] P. Martin and E. Salaün, "The true role of accelerometer feedback in quadrotor control," in *IEEE International Conference on Robotics and Automation (ICRA)*. IEEE, 2010, pp. 1623–1629.

[16] P. Pounds, R. Mahony, P. Hynes, and J. M. Roberts, "Design of a four-rotor aerial robot," in *Proceedings of the 2002 Australasian Conference on Robotics and Automation (ACRA)*. Australian Robotics & Automation Association, 2002, pp. 145–150.

[17] P. H. Zipfel, *Modeling and simulation of aerospace vehicle dynamics*. American Institute of Aeronautics and Astronautics, 2007.

[18] N. Chaturvedi, A. K. Sanyal, N. H. McClamroch, *et al.*, "Rigid-body attitude control," *Control Systems, IEEE*, vol. 31, no. 3, pp. 30–51, 2011.

[19] G. J. Balas, J. C. Doyle, K. Glover, A. Packard, and R. Smith, "μ-analysis and synthesis toolbox," *MUSYN Inc. and The MathWorks, Natick MA*, 1993.

[20] S. Lupashin, M. Hehn, M. W. Mueller, A. P. Schoellig, M. Sherback, and R. D'Andrea, "A platform for aerial robotics research and demonstration: The flying machine arena," *Mechatronics*, vol. 24, no. 1, pp. 41–54, 2014.